Influence of Cu column under-bump-metallizations on current crowding and Joule heating effects of electromigration in flip-chip solder joints

Y. C. Liang, W. A. Tsao, Chih Chen, Da-Jeng Yao, Annie T. Huang, and Yi-Shao Lai

Citation: Journal of Applied Physics **111**, 043705 (2012); doi: 10.1063/1.3682484
View online: http://dx.doi.org/10.1063/1.3682484
View Table of Contents: http://scitation.aip.org/content/aip/journal/jap/111/4?ver=pdfcov
Published by the AIP Publishing

Influence of Cu column under-bump-metallizations on current crowding and Joule heating effects of electromigration in flip-chip solder joints

Y. C. Liang,[1] W. A. Tsao,[1] Chih Chen,[1,a)] Da-Jeng Yao,[2] Annie T. Huang,[3] and Yi-Shao Lai[4]
[1]*Department of Materials Science and Engineering, National Chiao Tung University, Hsin-chu 30010, Taiwan*
[2]*Institute of Microelectromechanical System, National Tsing Hua University, Hsin-chu 30013, Taiwan*
[3]*Research Center for Applied Sciences, Academia Sinica, Taipei, 11529, Taiwan*
[4]*Central Laboratories, Advanced Semiconductor Engineering, Inc., Kao-hsiung 811, Taiwan*

(Received 12 July 2011; accepted 4 January 2012; published online 22 February 2012)

The electromigration behavior of SnAg solder bumps with and without Cu column under-bump-metallizations (UBMs) has been investigated under a current density of 2.16×10^4 A/cm^2 at 150 °C. Different failure modes were observed for the two types of samples. In those without Cu column UBMs, when SnAg solder bumps that had implemented 2 μm Ni UBMs were current stressed at 2.16×10^4 A/cm^2, open failure occurred in the bump that had an electron flow direction from the chip side to the substrate side. However, in those with Cu column UBMs, cracks formed along the interface of Cu_6Sn_5 intermetallic compounds and the solder on the substrate side in the Sn-3.0Ag–0.5Cu solder bump that had an electron flow direction from the substrate side to the chip side. A three-dimensional simulation of the current density distribution was performed in order to obtain a better understanding of the current crowding behavior in solder bumps. The current crowding effect was found to account for the void formation on both the chip and the substrate side for the two kinds of solder bumps. One more important finding, as confirmed by infrared microscopy, is that the alleviation of current crowding by Cu column UBMs also helped decrease the Joule heating effect in solder bumps during current stressing. Therefore, the measured failure time for the solder joints with Cu column UBMs appears to be much longer than that of the ones with the 2 μm Ni UBMs. © *2012 American Institute of Physics*. [doi:10.1063/1.3682484]

I. INTRODUCTION

For high-density packaging, the application of flip-chip solder joints has become the most important technology in the microelectronic industry.[1] In order to accommodate the performance requirements of portable devices, the input/output number continues to increase, and the size of the joints continues to shrink. This trend is behind the increase in current density and the temperature rise in solder joints, also known as the current crowding effect and Joule heating effect, respectively. These two effects cause serious reliability issues in flip-chip solder joints, such as electromigration (EM) and thermomigration.[2]

Several studies about the electromigration of flip-chip solder joints have been reported.[3–10] Current crowding especially has a strong effect at the entrance spot of the Al trace into the solder joint, and it is thus the main factor responsible for the failure near the chip/anode side in most solder joints.[4,5] However, the Joule heating effect also occurs during accelerated electromigration tests.[6–10] The temperature increase due to the Joule heating effect can be over 30 °C when a solder bump is stressed by a 1.0 A current.[5–7] Therefore, the Cu column under-bump-metallization (UBM), a structure with a thick UBM, was developed in order to alleviate both the current crowding and the Joule heating effect in flip-chip solder joints under normal operating conditions.[11] The operating temperature can affect the mean time to failure (MTTF) significantly, as depicted by Black's equation,[12]

$$\mathrm{MTTF} = \mathrm{A}\frac{1}{\mathrm{j}^{\mathrm{n}}}\exp\left(\frac{\mathrm{Q}}{\mathrm{kT}}\right), \tag{1}$$

where A is a constant, j is the current density in amperes per square centimeter, n is a model parameter for the current density, Q is the activation energy, k is Boltzmann's constant, and T is the average bump temperature in degrees Kelvin.

Only a few studies have been reported regarding the EM failure mechanism for solder joints with Cu column UBMs.[13–15] Nah *et al.* reported electromigration in flip-chip solder joints with 50 μm thick Cu columns, and they found that the Cu columns can relieve the current crowding effect in solder.[13] Lai *et al.* investigated the MTTF and failure mechanism of electromigration in solder joints with 62 μm thick Cu columns, and they found that the MTTF of the joints was enhanced by the thick Cu columns.[14] Xu *et al.* reported that electromigration accelerated the consumption rate of the Cu columns and transformed almost the entire solder into intermetallic compounds (IMCs).[15] However, no study has addressed the Joule heating effect of solder joints with Cu UBMs. In this study, we investigate EM failures in solder bumps with 64 μm thick Cu column UBMs. Electromigration tests were also performed in solder joints with 2 μm thick Ni UBMs for comparison. The wiring circuits are the same for both sets of solder joints. Therefore, this study provides a direct comparison of the failure mode and

a)Author to whom correspondence should be addressed. Electronic mail: chih@mail.nctu.edu.tw.

thermo-electrical characteristics of regular solder joints and solder joints with Cu column UBMs.

II. EXPERIMENTAL

In order to investigate the influence of Cu columns on current crowding and Joule heating effects, two types of flip chip solder joints were tested: one type has traditional solder joints with 2 μm thick Ni UBMs, and the other type has an addition of 64 μm thick Cu column UBMs followed by a 4 μm thick Ni layer.

The test vehicles were 13.5 mm $\times$ 13.5 mm $\times$ 1.39 mm flip-chip packages involving a 3.8 mm $\times$ 3.8 mm $\times$ 0.73 mm silicon chip interconnected to a substrate. The pitch between adjacent solder joints was 270 μm. The diameters of the UBM opening and the passivation opening were 110 μm and 90 μm, respectively. A printed solder of Sn-2.6Ag and Sn-3.0Ag–0.5Cu solder were formed on the chip side. The substrate pad metallization featured the solder on pad (SOP) surface treatment, i.e., with printed Sn-3.0Ag–0.5Cu pre-solder on the Cu pad surface. The printed solder and the SOP were then reflowed together to become lead-free solder bumps as schematically shown in Figs. 1(a) and 1(b). For electromigration tests, the stressing condition was 2.16×10^4 A/cm^2 at 150 °C.

The microstructure and composition were examined using a JEOL 6500 field-emission scanning electron microscope (SEM) and energy dispersive spectroscopy (EDS), respectively. The IMC $(Cu,Ni)_6Sn_5$ was formed at the interface of the Ni layer and the solder on the chip side, whereas Cu_6Sn_5 without Ni dissolution was formed at the interface of the solder and the Cu metallization layer on the substrate side. In addition, Ag_3Sn IMCs were formed dispersedly in the solder bumps.

In order to investigate the Joule heating issue during current stressing, infrared (IR) microscopy was employed. Solder joints were completely enclosed by a Si chip, underfill, and a polymer substrate, so it was difficult to examine the temperature inside solder joints directly. To overcome this difficulty, samples were polished laterally close to a point near the center, and the temperature distribution inside the solder bump was measured directly with an IR microscope at various stressing conditions. Prior to current stressing, the emissivity of the specimen was calibrated at 100 °C. After calibration, solder joints were powered by a desired current. Temperature measurement was then performed to record the temperature map distribution at a constant rate. The temperatures in the solder joints were mapped by a Quantum Focus Instruments thermal infrared microscope, which has a 0.1 °C temperature resolution and a 2 μm spatial resolution.

III. SIMULATION

Three-dimensional (3D) finite element analysis was employed in order to simulate the current density distribution in the solder joints. The model included two solder joints, an Al trace, and two Cu lines as shown in Fig. 2, in which the direction of the electron flow is shown by two of the arrows. The dimensions of the Al trace, the pad opening, and the Cu line were identical to those in the real flip-chip samples. The IMCs formed between the UBM and the solder were also considered in the simulation models. Layered IMCs of Cu_6Sn_5 were used in this simulation so as to avoid difficulty in the mesh. The resistivity values of the materials used in the simulation are listed in Table I. The resistivity of Sn-2.6Ag cannot be found in the literature; therefore, we adopted a resistivity of Sn-3.0Ag–0.5Cu for the solder, which should be very close to the resistivity of Sn-2.6Ag. The model used in this study was a SOLID5 8-node hexahedral coupled field element, using ANSYS simulation software.

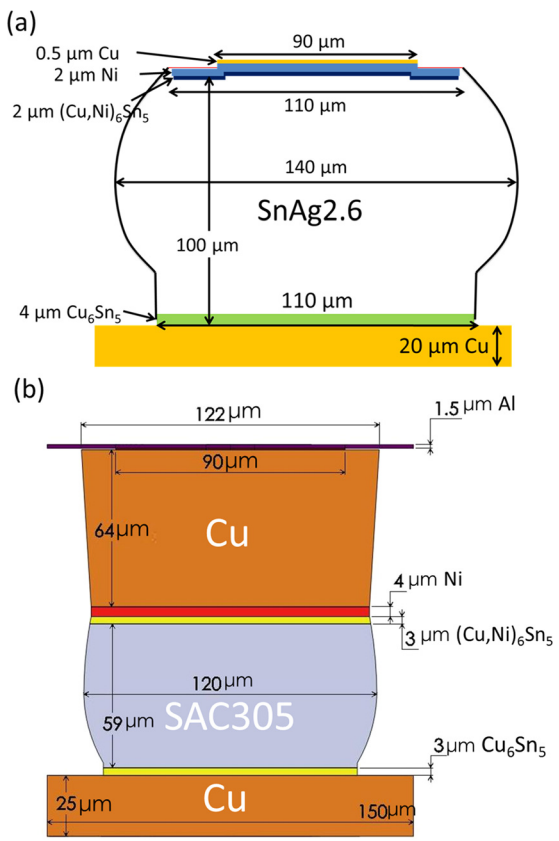

FIG. 1. (Color online) Schematics of the flip-chip solder joints with (a) a Ni UBM and (b) a Cu column UBM in this study.

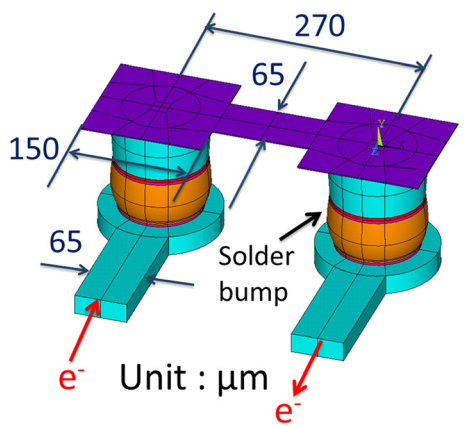

FIG. 2. (Color online) The simulation model for one pair of the flip-chip solder joints. The arrows show the direction of the electron flow.

TABLE I. The properties of materials used in the simulation model.

Materials	Resistivity at 20 °C ($\mu\Omega$ cm)
Al	3.2
Cu	1.7
Ni	6.8
Cu_6Sn_5	17.5
Sn-3.0Ag–0.5Cu solder	12.3

IV. RESULTS AND DISCUSSION

The case without a Cu column UBM is presented here first. Figure 3(a) illustrates the cross-sectional SEM image of a solder bump with a Ni UBM before EM tests. Figures 3(b) and 3(d) show the cross-sectional SEM images of solder bumps with Ni UBMs after upward and downward current stressing of 2.16×10^4 A/cm^2 at 150 °C for 42.7 h. The current density was calculated based on the area of the passivation opening on the chip side. Open failure occurred after 42.7 h of current stressing, and the damage in the Al trace between two solder bumps can be observed via IR microscopy. When the direction of the electron flow was from the substrate side to the chip side, as shown in Fig. 3(b), some of the Cu metallization layer on the substrate side was consumed and reacted with solder to form Cu_6Sn_5 IMCs. A slight amount of Cu_6Sn_5 IMCs in the solder bump near the substrate side was aligned with the direction of electron flow because of the electromigration effect in the solder joint. A crack formed along the chip/solder interface, which may be attributed to polishing during sample preparation for cross-sectional SEM observation. Additionally, some voids were observed in the Al trace on the chip side, as labeled in Fig. 3(b). Some of the voids were filled with Sn atoms. Figure 3(c) shows the EDS analysis for location *A* in Fig. 3(b), and the results indicate that the element there was almost pure Sn (we discuss this interesting point later). When the direction of the electron flow was from the chip side to the substrate side, as shown in Fig. 3(d), the solder melted because of a serious Joule heating effect. The underfill layer was also damaged. However, the EM failure mode of the solder joints with Cu columns is quite different. Figure 4(a) shows a cross-sectional SEM image of a solder bump with a Cu column UBM before EM tests. Figures 4(b) and 4(c) show cross-sectional SEM images of solder bumps with Cu column UBMs after upward and downward current stressing of 2.16×10^4 A/cm^2 at 150 °C for 286.5 h. During this period of current stressing time, the total resistance, which includes two solder joints and the Al trace, is raised by 50 mΩ, from 145 mΩ to 195 mΩ. When the direction of the electron flow was from the substrate side to the chip side, as shown in Fig. 4(b), voids about 84.7 μm long could be observed clearly at the interface of Cu_6Sn_5 IMCs and the solder on the substrate side. The voids in the middle of the solder may be attributed to the reflow process. This crack was the main reason for the resistance increase during the failure. Similar to the results for the solder joint with a 2 μm Ni UBM shown in Fig. 3(b), extensive dissolution of the Cu layer on the substrate side took place, resulting in the massive formation of Cu-Sn

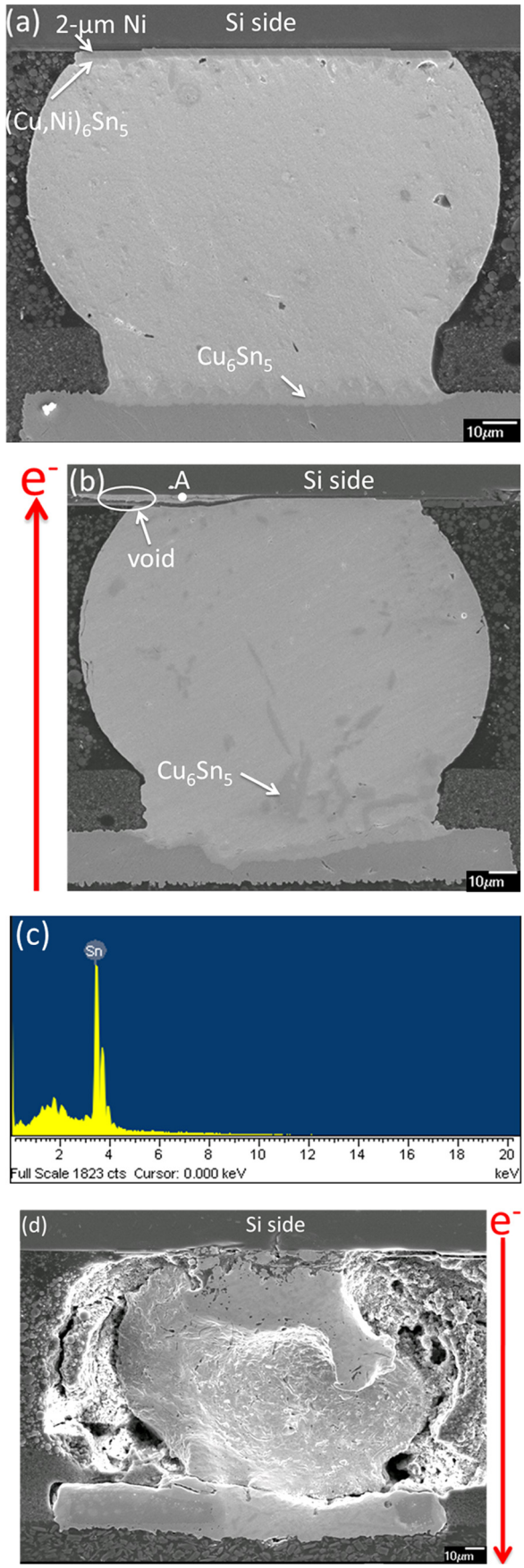

FIG. 3. (Color online) Cross-sectional SEM images of a solder bump with a 2 μm Ni UBM stressed at 2.16×10^4 A/cm^2 at 150 °C for (a) 0 h, (b) 42.7 h with upward electron flow, (c) EDS analysis at point A in (b), and (d) 42.7 h with downward electron flow.

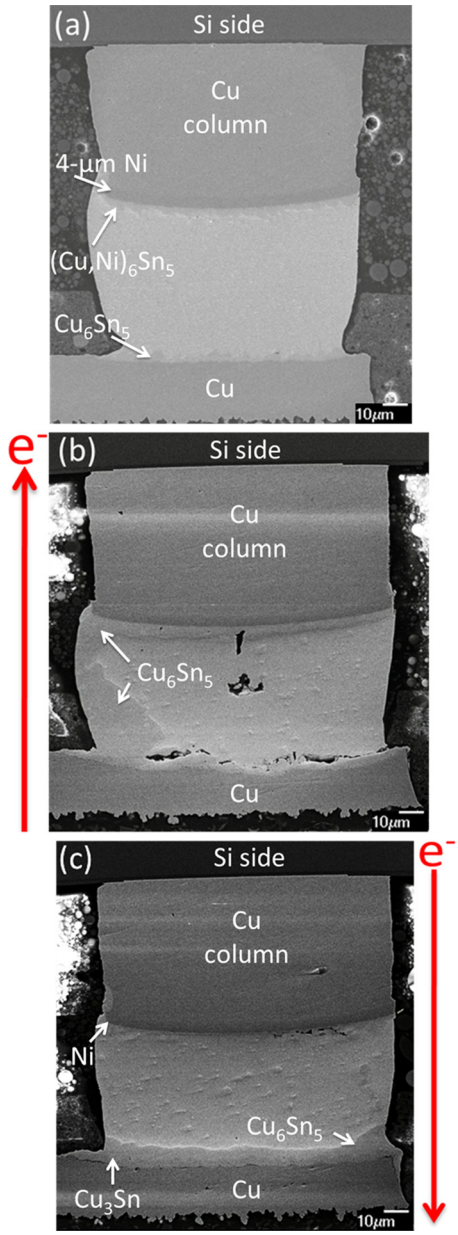

FIG. 4. (Color online) Cross-sectional SEM images of a solder bump with a Cu column UBM stressed at 2.16×10^4 A/cm^2 at 150 °C for (a) 0 h, (b) 286.5 h with upward electron flow, and (c) 286.5 h with downward electron flow.

IMCs in the solder. Yet no voids are found on the substrate side in Fig. 3(b). Ke *et al*. reported two failure mechanisms that might occur in solder joints with Cu UBMs: void formation and Cu dissolution.[16] It is not clear at this moment why voids did not form in the solder joints in Fig. 3(b).

When the direction of the electron flow was from the chip side to the substrate side, as shown in Fig. 4(c), the IMCs at the interface of the Ni layer and the solder became thinner, whereas the IMCs at the interface of the solder and the Cu metallization layer on the substrate side became thicker because of the polarity effect. A void about 28 μm long formed in the top-right-hand corner in the solder bump, and some Kirkendall voids can be observed at the interface of Cu_3Sn IMCs and the Cu metallization layer on the substrate side. The Cu column and the Ni layer beneath remained intact within our experimental time frame.

The current crowding effect plays a crucial role in the electromigration failure of solder joints. Because the current density in the Al trace is typically one or two orders in magnitude larger than that in the solder, current crowding occurs at the entrance point of the Al trace into the solder joint. Figure 5 depicts a 3D simulation of the current density distribution in the solder bump with Ni UBMs. The applied current was 1.5 A from the chip side to the substrate side, which resulted in a current density of 1.54×10^6 A/cm^2 in the Al trace. The calculated average current density was 2.16×10^4 A/cm^2 based on the area of the passivation opening on the chip side. However, due to the current crowding effect, the maximum current density inside the solder bump was as high as 7.8×10^4 A/cm^2, as shown in Fig. 5.

With a Cu column UBM, a more uniform distribution of current density was obtained in the solder bump, as shown in Figs. 6(a) and 6(b). As in Fig. 5, the applied current was 1.5 A from the chip side to the substrate side. The maximum current density in the Cu column was 1.0×10^6 A/cm^2. It can be seen that the current crowding effect still occurs in the Cu column UBM near the entrance of the Al trace into the solder joint. However, because Cu has a much higher melting point than SnAg solder (Cu: 1084 °C; SnAg: 221 °C), there was little EM damage in the Cu in the present stressing condition. The Cu column UBM is thick enough that the solder is kept away from the current crowding region, and the maximum current density in the solder bump dramatically decreases to 4.0×10^4 A/cm^2, which is only 51% of the maximum current density inside the solder bump with the 2 μm Ni UBM. In other words, the current flow spreads out and becomes more uniform before reaching the solder bump when a Cu column UBM is utilized. As a result, instead of being located on the chip side, the current crowding region in the solder bump with Cu column UBMs is actually located on the substrate side. This result agrees with the phenomenon observed in Fig. 3(d) and Fig. 4(b). The main electromigration-induced

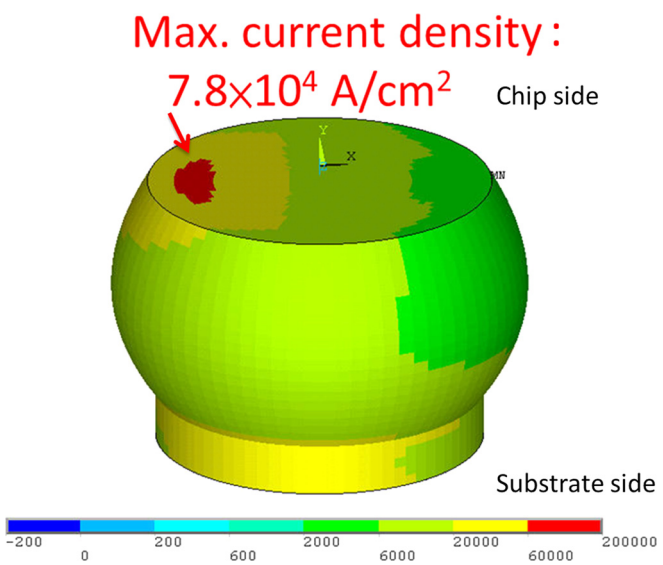

FIG. 5. (Color online) Simulation results for current density distribution in the solder bump with a 2 μm Ni UBM when powered by 1.5 A.

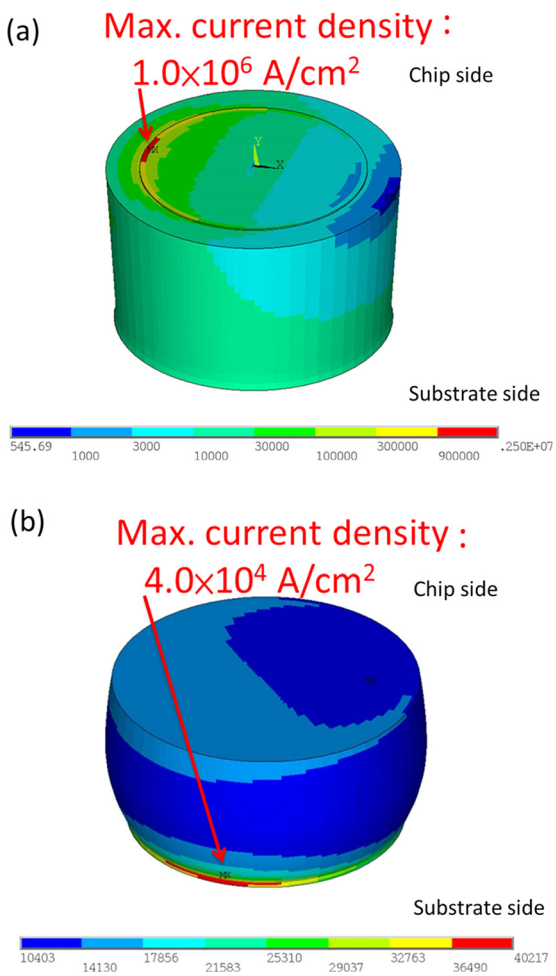

FIG. 6. (Color online) Simulation results for the current density distribution in (a) the Cu column UBM and (b) the solder bump beneath when powered by 1.5 A.

damage position in the solder bump moved from the chip side to the substrate side because of the existence of Cu column UBMs.

The existence of Cu column UBMs also has an influence on the Joule heating effect in the solder bump. Current stressing was carried out at a temperature of 100 °C on a hotplate. Figure 7 shows that the temperature increases in solders with 2 μm Ni UBMs and Cu column UBMs during current stressing as a function of applied current and current density. Current stress was applied to solder joints with a current density in the range of 2.88×10^3 A/cm^2 to 2.30×10^4 A/cm^2 in the passivation opening. Figures 8(a) and 8(b) show the temperature distribution of the cross-sectioned solder bump with Ni UBMs and Cu column UBMs, respectively, during current stressing of 2.30×10^4 A/cm^2 at 100 °C (the temperature scale bars are shown at the bottom of the figures). The average temperature increases were 17.9 °C and 14.4 °C in solder bumps with Ni UBMs and Cu column UBMs, respectively. In this study, the mean temperature was determined by averaging the values of 1000 pixels surrounding an approximately (65×40) μm^2 rectangular area in the center of the solder bump. Under the same current density, the alleviation of current crowding by the Cu column UBM consequently decreased the temperature rise in the solder bump. It is also

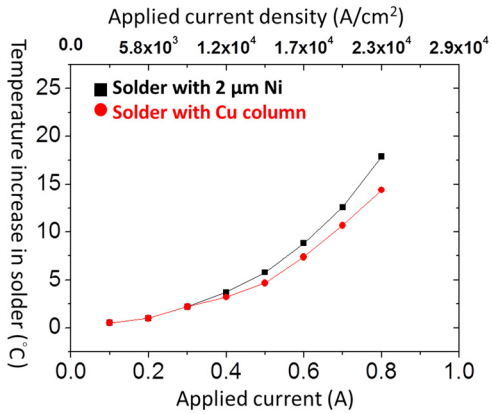

FIG. 7. (Color online) Temperature increases in solders with 2 μm Ni UBMs and Cu column UBMs during current stressing as a function of applied current and current density.

known that an Al trace under current stressing is a stable heating source, and the heat generated by the Joule heating of the Al trace should always flow from a high temperature region toward a low temperature region. We have noticed, however, as shown in Fig. 8(b) for the case of a Cu column UBM, that the temperature increase in the Cu column UBM seems to be lower than that in the solder bump. This

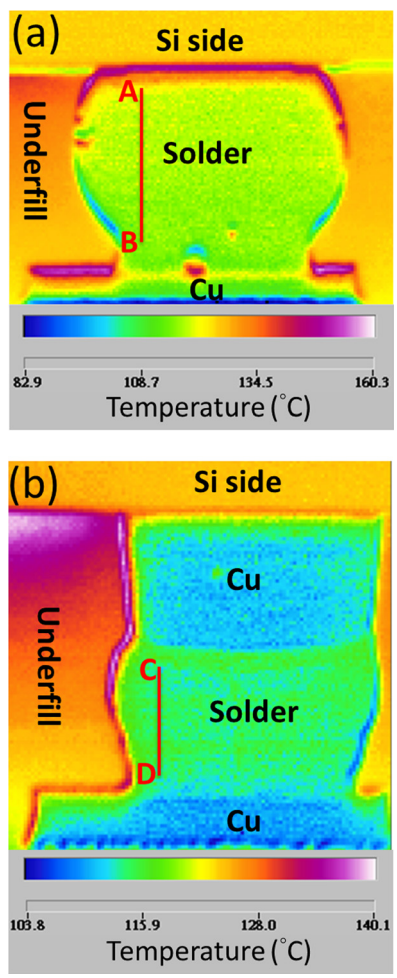

FIG. 8. (Color online) IR images showing the temperature distribution in solder bumps with (a) a 2 μm Ni UBM and (b) a Cu column UBM during current stressing of 2.30×10^4 A/cm^2 at 100 °C.

seemingly contradictory result actually comes from the difference between "thermal gradients" and "radiance gradients." Because Cu and solder's surface characteristics are different, what was measured does not represent the real temperature difference between the Cu column UBM and the solder joint. Nevertheless, in general, the temperature increase in various solder bumps can still been compared, because the emissivity of solder is consistent.

The Cu column also decreases the thermal gradient in the solder during high-current stressing. Figure 9(a) shows the temperature profile along the $\overline{AB}$ line in Fig. 8(a). The temperature difference is 6.0 °C along the line, and the calculated thermal gradient is 600 °C/cm. Here, the thermal gradient is defined as the temperature difference between the two ends of the line divided by the length of the line. However, there is no obvious thermal gradient in the solder joint with the Cu column under the same stressing condition. Figure 9(b) presents the temperature profile along the $\overline{CD}$ line in Fig. 8(b). No obvious temperature difference is found across the $\overline{CD}$ line; therefore, thermomigration might be relieved in the joints with a Cu column.

The solder joints with a Cu column UBM have a longer failure time than the ones with a 2 μm Ni UBM, because the Cu column helps reduce the current density in the solder and the Joule heating effect. As described by Black's equation in Eq. (1), the MTTF can be prolonged when the current density and the temperature in solder can be reduced, provided the activation energy remains the same. In general, the value n in Eq. (1) is close to 2, which means the MTTF will double if the current density in solder is reduced to half of its original value.[6] As shown in Fig. 5, the maximum current density inside the solder bump with a 2 μm Ni UBM is as high as 7.8×10^4 A/cm^2, whereas the maximum current density in the solder bump with a 64 μm Cu column dramatically decreases to 4.0×10^4 A/cm^2, which is only 51% of the maximum current density inside the solder bump with the 2 μm Ni UBM. Therefore, the lower current density results in a longer MTTF of the solder bump with the Cu column. In addition, the MTTF increase exponentially when the real temperature in solder joints decreases. The results in Fig. 8 indicate that the Cu column reduces the Joule heating effect. Thus, the real temperature in the solder bump with the Cu column appears to be lower than that in the solder joint with a 2 μm Ni UBM, which also increases the MTTF of the solder joint with the Cu column. For the solder joints with 2 μm Ni UBMs, open failure took place at 42.7 h when they were subjected to a current density of 2.16×10^4 A/cm^2 at 150 °C, as shown in Fig. 3. However, for the solder joint with the Cu column, the resistance increased only 50 mΩ after 286.5 h at the same stressing condition. The thick Cu column keeps the solder away from the region with a high current density. In addition, it possesses a high thermal conductivity, so that the heat generated by the Joule heating effect can be conducted away efficiently. Moreover, the thick Cu column also keeps the solder away from the hot-spot region,[17] and therefore the temperature in the solder is reduced.

The voids in the Al trace in Fig. 3(b) were caused by electromigration. It is reported that electromigration in the Al trace also occurs when the current density is larger than 1.0×10^6 A/cm^2 at 150 °C.[18,19] In the present study, the current density is 1.54×10^6 A/cm^2 in the Al trace, and thus voids can form in the cathode end of the Al trace, as labeled in the figure. Once voids have formed in the Al trace, the Sn atoms might be pushed into the voids by the upward electron flow.

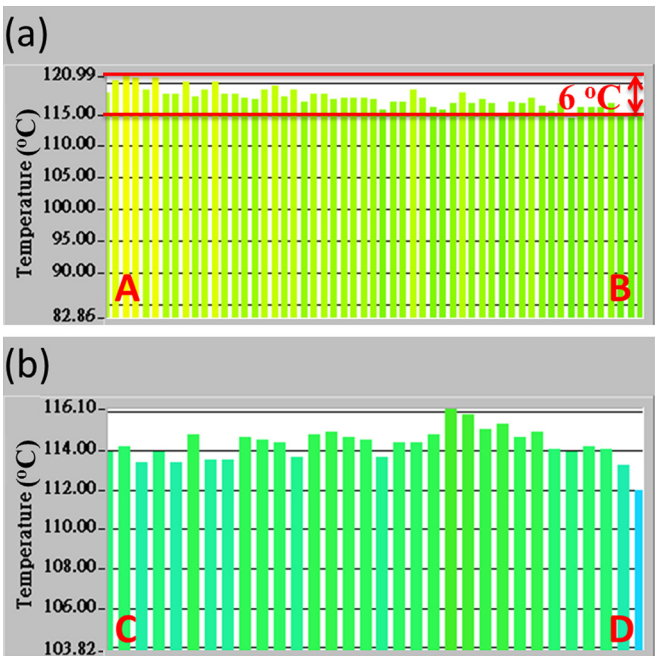

FIG. 9. (Color online) (a) The temperature profile along the $\overline{AB}$ line in Fig. 8(a). (b) The temperature profile along the $\overline{CD}$ line in Fig. 8(b).

V. CONCLUSIONS

Electromigration-induced failures in SnAg solder bumps with and without Cu column UBMs have been investigated under a current density of 2.16×10^4 A/cm^2 at 150 °C. When SnAg solder bumps with 2 μm Ni UBMs were stressed at 2.16×10^4 A/cm^2, open failure occurred in the bump that had an electron flow direction from the chip side to the substrate side. However, when Sn-3.0Ag–0.5Cu solder bumps with Cu column UBMs were stressed at 2.16×10^4 A/cm^2, cracks formed along the interface of Cu_6Sn_5 IMCs and the solder on the substrate side. The three-dimensional simulation of the current density distribution supports the contention that the current crowding effect was responsible for the failure on both the chip and the substrate side for the two kinds of solder bumps. As confirmed via IR microscopy, the alleviation of current crowding by the Cu column UBMs also helped decrease the Joule heating effect in the solder bump during current stressing. Therefore, the solder joints with Cu column UBMs have a higher EM resistance than the traditional flip-chip solder joints.

ACKNOWLEDGMENTS

Financial support from the National Science Council, Taiwan, under Contract No. NSC 98-2221-E-009-036-MY3 is acknowledged.

[1]K. N. Tu, J. Appl. Phys. **94**, 5451 (2003).
[2]C. Chen, H. M. Tong, and K. N. Tu, Annu. Rev. Mater. Res. **40**, 531 (2010).
[3]C. Y. Liu, C. Chen, C. N. Liao, and K. N. Tu, Appl. Phys. Lett. **75**, 58 (1999).
[4]E. C. C. Yeh, W. J. Choi, and K. N. Tu, Appl. Phys. Lett. **80**, 4 (2002).
[5]T. L. Shao, Y. H. Chen, S. H. Chiu, and C. Chen, J. Appl. Phys. **96**(8), 4518 (2004).
[6]W. J. Choi, E. C. C. Yeh, and K. N. Tu, J. Appl. Phys. **94**(9), 5665 (2003).
[7]H. Ye, C. Basaran, and D. Hopkins, Appl. Phys. Lett. **82**, 7 (2003).
[8]S. H. Chiu, T. L. Shao, and C. Chen, Appl. Phys. Lett. **88**, 022110 (2006).
[9]S. W. Liang, Y. W. Chang, and C. Chen, Appl. Phys. Lett. **88**, 172108 (2006).
[10]H. Y. Hsiao and C. Chen, Appl. Phys. Lett. **90**, 152105 (2007).
[11]S. W. Liang, T. L. Shao, C. Chen, E. C. C. Yeh, and K. N. Tu, J. Mater. Res. **21**, 1 (2006).
[12]J. R. Black, IEEE Trans. Electron Devices **16**, 338 (1969).
[13]J. W. Nah, J. O. Suh, K. N. Tu, S. W. Yoon, V. S. Rao, V. Kripesh, and F. Hua, J. Appl. Phys. **100**, 123513 (2006).
[14]Y. S. Lai, Y. T. Chiu, and J. Chen, J. Electron. Mater. **37**, 1624 (2008).
[15]L. Xu, J. K. Han, J. J. Liang, K. N. Tu, and Y. S. Lai, Appl. Phys. Lett. **92**, 262104 (2008).
[16]J. H. Ke, T. L. Yang, Y. S. Lai, and C. R. Kao, Acta Mater. **59**, 2462 (2011).
[17]H. Y. Hsiao, S. W. Liang, M. F. Ku, C. Chen, and D. J. Yao, J. Appl. Phys. **104**, 033708 (2008).
[18]F. Y. Ouyang, K. N. Tu, C. L. Kao, and Y. S. Lai, Appl. Phys. Lett. **90**, 211914 (2007).
[19]S. W. Liang, S. H. Chiu, and C. Chen, Appl. Phys. Lett. **90**, 082103 (2007).